Atmos. Meas. Tech. Discuss., 2, 37–86, 2009
www.atmos-meas-tech-discuss.net/2/37/2009/

Atmospheric Measurement Techniques Discussions

Atmospheric Measurement Techniques Discussions is the access reviewed discussion forum of *Atmospheric Measurement Techniques*

Intercomparison of stratospheric ozone and temperature profiles during the October 2005 Hohenpeissenberg Ozone Profiling Experiment (HOPE)

W. Steinbrecht[1], T. J. McGee[2], L. W. Twigg[2], H. Claude[1], F. Schönenborn[1], G. K. Sumnicht[2], and D. Silbert[2]

[1]Meteorologisches Observatorium, Deutscher Wetterdienst, Hohenpeißenberg, Germany
[2]NASA Goddard Space Flight Center, Greenbelt MD, USA

Received: 5 November 2008 – Accepted: 8 December 2008 – Published: 12 January 2009

Correspondence to: W. Steinbrecht (wolfgang.steinbrecht@dwd.de)

Published by Copernicus Publications on behalf of the European Geosciences Union.

Abstract

Thirteen clear nights in October 2005 allowed successful intercomparison of the stationary lidar operated since 1987 by the German Weather Service (DWD) at Hohenpeissenberg (47.8° N, 11.0° E) with the Network for the Detection of Atmospheric Composition Change (NDACC) travelling standard lidar operated by NASA's Goddard Space Flight Center. Both lidars provide ozone profiles in the stratosphere, and temperature profiles in the strato- and mesosphere. Additional ozone profiles came from on-site Brewer/Mast ozonesondes, additional temperature profiles from Vaisala RS92 radiosondes launched at Munich (65 km north-east), and from operational analyses by the US National Centers for Environmental Prediction (NCEP). The intercomparison confirmed a low bias for ozone from the DWD lidar in the 33 to 43 km region, by up to 10%. This bias is caused by the DWD ozone algorithm. It will be removed in a future version. Between 20 and 33 km, agreement between both lidars, and ozonesondes below 30 km, is good with ozone differences less than 3 to 5%. Results are consistent with previous comparisons of the DWD lidar with SAGE, GOMOS and other satellite instruments. The intercomparison did uncover a 290 m upward shift of the DWD lidar data. When this shift is removed, agreement with ozone from the NASA lidar improves below 20 km, with remaining differences usually less than 5%, and not statistically significant. Precision (repeatability) for the lidar ozone data is better than 5% between 20 and 40 km altitude, dropping to 10% near 45 km, and 50% near 50 km. Temperature from the DWD lidar has a 1 to 2 K cold bias from 30 to 65 km against the NASA lidar, and a 2 to 4 K cold bias against radiosondes and NCEP. This is consistent with previous intercomparisons against NCEP or radiosondes. The cold bias against the NASA lidar disappears when the DWD lidar data are corrected for the afore-mentioned 290 m range error, and more appropriate values for the Earth's gravity acceleration are used. Temperature precision (repeatability) for the DWD lidar is better than 2 K between 30 and 50 km , decreasing to 10 K near 70 km. It is over-estimated by the current DWD algorithm, and should be reduced by a factor of 2.2 (e.g. from 22 K to

10 K near 70 km). Temperature and ozone variations are tracked well by both lidars, by ozone- and radiosondes, and by NCEP analyses. Correlations exceed 0.8 to 0.9 at most stratospheric levels. They decrease at levels above 40 km, especially for ozone or NCEP temperature. The ozone and temperature bias of the DWD lidar does not appear to have changed over the years. Long-term records of ozone and temperature from the DWD lidar should be consistent. Nevertheless, the HOPE intercomparison was instrumental in uncovering several long-standing errors. These need to be fixed and the entire DWD lidar data record needs to be reprocessed.

1 Introduction

Around 1990, the International Network for the Detection of Stratospheric Change (NDSC, http://www.ndsc.ncep.noaa.gov) was formed to provide a consistent, standardized set of long-term measurements of stratospheric trace gases, particles, and physical parameters via a suite of globally distributed sites. Within the NDSC, which was expanded and renamed Network for the Detection of Atmospheric Composition Change (NDACC) in 2006, lidars (= laser radars) are key instruments for measuring the stratospheric ozone and temperature profile. Lidar measurements of ozone and temperature are self-calibrating, in principle (e.g., Hauchecorne and Chanin, 1980; Megie et al., 1985; Carswell et al., 1991). This makes them especially suited for long-term monitoring.

An important aspect of NDACC are dedicated instrument intercomparison campaigns, where several instruments are co-located to measure in close spatial and temporal vicinity for an intensive period of days to weeks. Examples are the 1989 Stratospheric Ozone Intercomparison Campaign at Table Mountain (Margitan et al., 1995), the 1995 Ozone Profiler Assessment at Lauder (McDermid et al., 1998a,b), or the 1997 intercomparison at Haute Provence (Braathen et al., 2004). Keckhut et al. (2004) give an overview. In many NDACC lidar intercomparisons, the mobile lidar operated by NASA's Goddard Space Flight Center (NASA-GSFC) has served as the travelling

standard. This system has been modified and improved (McGee et al., 1991, 1993, 1995a; Gross et al., 1997), whereas the stationary lidar run since September 1987 by the German Weather Service (DWD) at Hohenpeissenberg (47.8° N, 11.0° E) has undergone only very few modifications over the years, most notably a change of the photon-counters in January 1995, and a change of the interference filters in November 1998. The DWD lidar has provided one of the longer NDACC time series (Geh, 1987; Claude et al., 1994), but has so far not participated in a formal NDACC on-site intercomparison. Intercomparisons with local ozonesondes, and satellite measurements, however, have been done on many occasions (Steinbrecht et al., 1997, 2006). In October 2005, the mobile NASA-GSFC lidar was finally deployed at Hohenpeissenberg for intercomparison in the Hohenpeissenberg Ozone Profiling Experiment (HOPE).

The present paper reports main results of this HOPE intercomparison, and puts them into the context of previous intercomparisons. Our focus is on validation of the DWD lidar. Ozone and temperature profiles from the two lidars, from ozone- and radiosondes and from US National Centers for Environmental Prediction (NCEP) temperature analyses are compared. The paper is organized as follows: Section 2 describes the two lidar systems and their processing algorithms. Section 3 gives details of the HOPE campaign. Section 4 presents the intercomparison results. Section 5 discusses important errors uncovered by the HOPE intercomparison, and shows how they affect ozone and temperature profiles from the DWD lidar. Conclusions are drawn in Sect. 6.

2 Lidar hardware, principle, and processing

Figure 1 gives a schematic of the DWD lidar at Hohenpeissenberg, and Table 1 summarizes the main characteristics of the DWD and NASA lidar systems. A Xenon Chloride excimer laser generates pulses of intense ultraviolet radiation at 308 nm. These are focused into a Raman cell, filled with pure hydrogen. Near the focus, stimulated Raman scattering by the hydrogen molecules generates a light pulse at 353 nm (and other wavelengths), which travels simultaneously and in the same direction as the original

308 nm pulse (e.g., Werner et al., 1983). Both pulses pass through a beam expanding telescope (10x expansion) and are transmitted vertically up into the atmosphere. A small fraction of the light is scattered back by air molecules in the atmosphere. This returned light is collected by the large primary mirror of the receiver. Inside the receiver's detector unit, a dichroic mirror separates the two emitted wavelengths. Narrowband interference filters reject skylight and the unwanted opposite wavelength. Returned photons are then detected by two photomultipliers (PM1, PM2) in photon counting mode. Discriminators separate noise from true photon pulses and multichannel scalers count the returned photons (= pulses) as a function of time (= range). A crucial component is the bow-tie shaped chopper blade. It is rotating at high speed across the telescope focus. Laser pulses are synchronized to this chopper blade, so that the very intensive return signal from low altitudes (= early times) is blocked (Werner et al., 1983; Geh, 1987; Steinbrecht et al., 1989). The chopper is crucial to avoid photomultiplier overload and unwanted after effects like signal induced noise (Iikura et al., 1987; Williamson and Young, 2000).

The conceptual setup of the NASA lidar is similar (McGee et al., 1995a). However, instead of a Raman cell, the NASA lidar uses a second laser to generate pulses at 355 nm (Nd:YAG 3rd harmonic). Also, instead of 2 detector channels only (PM1, PM2), the NASA lidar uses 8 detector channels. This allows simultaneous recording of return signals at 308 and 355 nm with full intensity and with intensity reduced by a grey filter (= HI and LOW channels), as well as recording of return signals from vibrational Raman scattering by nitrogen (332 nm, 387 nm with HI and LOW channels), plus return signals from vibrational Raman scattering by water vapour (407 nm). The NASA system has been upgraded several times since its beginnings in 1990, whereas the DWD system has intentionally been kept close to the original status from 1987.

Typical atmospheric return signals are given in Fig. 2, for the night of 27 to 28 October 2005. In this night, the NASA lidar measured from 18:18 to 03:59 UT, the DWD lidar from 19:25 to 04:21 UT. The DWD lidar uses 300 m range bins below 80 km and 17 km range bins above. The NASA lidar uses 15 m range bins, but for the plot in Fig. 2

these have been summed to 300 m range bins. Noteworthy in Fig. 2 are the high dynamic range, more than 5 orders of magnitude, and the low number of photons counted at high altitudes. At 70 km, for example, the DWD system photon count rate is only about 100 Hz, i.e. only 1 photon is counted every 10000 laser shots in a 1 µs (=150 m) range bin. The much higher count rates of the NASA lidar show the benefits of a larger receiver mirror, more powerful lasers, better photomultipliers, and other technical improvements.

The lidar return signal P_{off} at 353 nm (or 355 nm) is not absorbed by ozone. However, it contains information about the atmospheric density and temperature profiles. The return signal P_{on} at 308 nm behaves similar, but is additionally absorbed by ozone (absorption cross-section σ_{O_3}). The absorption leads to the more rapid decay of the 308 nm signals with altitude z. In Fig. 2 this is seen best for the DWD return signals near 25 km. Essentially, comparison of the slopes of the logarithm of the return signals at 308 and 353 nm, $P_{\text{on}}(z)$ and $P_{\text{off}}(z)$ (blue and red lines in Fig. 2), gives the ozone number density profile $n_{O_3}(z)$ (e.g., Megie et al., 1985; Carswell et al., 1991; Steinbrecht and Carswell, 1995):

$$n_{O_3}(z) = \frac{1}{2\sigma_{O_3}} \frac{d}{dz} \ln \frac{P_{\text{off}}(z)}{P_{\text{on}}(z)} \tag{1}$$

Numerical calculation of the derivative d/dz in Eq. (1) becomes problematic at high altitudes, where the return signals are noisy (statistical noise due to the few counted photons). Taking the derivative then tends to result in very noisy ozone profiles. To reduce this problem, derivative filters in ozone processing algorithms use information from many range bins:

$$\frac{df}{dz}(z_0) = \sum_{i=-k}^{k} w(i) f(z_i) \tag{2}$$

Choosing width k and weights $w(i)$ of a derivative filter always requires a trade-off between low noise and coarse range resolution (large k), or high noise and fine range

resolution (small k). The choice depends on the characteristics of the specific lidar system, and on the scientific objectives of the measurements. Historically, the different NDACC lidar groups have chosen different derivative filters and have developed their own processing algorithms (see Godin et al., 1999, for an intercomparison). Nearly all groups use a narrow filter with fine range resolution at lower altitudes, where photon counts are high, and wider filters with coarse range resolution at high altitudes, where photon counts are low. A wider filter (large k) uses more altitude channels, thus more counted photons. This reduces statistical noise. For three selected altitude levels, Fig. 3 shows the derivative filters $w(i)$ for the DWD and NASA ozone processing algorithms. Near 25 km altitude, both algorithms use similar filter widths, and filter shapes are comparable. At 35 and 45 km, however, the DWD derivative filter is much wider and also has a clearly different shape from the NASA filter. The DWD algorithm is equivalent to first smoothing $f(z)$ with a Gaussian, and then taking the slope between the two points above and below the desired altitude z_0 (Steinbrecht et al., 1997). The NASA derivative filter is implemented by fitting a straight line (linear ramp) to $f(z)$, in a given window (1st or 2nd order Savitzky Golay filter, e.g. Press et al., 1992). The width of this window is increased with increasing altitude. The slope of the fitted line gives the derivative $df(z)/dz$.

A simple way to define the range resolution Δz for a derivative filter $w(i)$ is to use the distance between the "center" of the positive and negative lobes of the derivative filter at z_0 (compare Fig. 3).

$$\Delta z = \frac{\sum_{i=-k}^{k} w(i)(z_i - z_0)}{\sum_{i=-k}^{k} |w(i)|} \tag{3}$$

The resulting range resolutions Δz for the filters at 35 and 45 km are indicated by the dashed lines in Fig. 3.

The change of the range resolution Δz (defined by Eq. (3)) with altitude is shown in Fig. 4 for the NASA and DWD ozone processing algorithms. Below 30 km altitude, both algorithms have similar fine range resolution, between 0.5 and 1.5 km. Above

25 km, however, the range resolution for the DWD algorithm becomes coarser very fast, changing from 1.5 km near 30 km to almost 9 km near 40 km. For the NASA algorithm, the increase is smaller and more gradual, from 1.5 km near 30 km to 3 km near 50 km altitude. The much coarser range resolution of the DWD ozone algorithm is used to counteract the much lower photon count rates of this system (compare Fig. 2).

In order to derive the temperature profile, NASA and DWD processing both follow the method of Hauchecorne and Chanin (1980). Above the stratospheric aerosol layer, i.e. above about 30 km, the unabsorbed return signal $P_{\text{off}}(z)$ (at 353 or 355 nm) is proportional to molecular density $n_{\text{air}}(z)$:

$$n_{\text{air}}(z) \propto P_{\text{off}}(z) z^2 \tag{4}$$

Assuming hydrostatic equilibrium, and given the acceleration by Earth's gravity $g(z)$, as well as the mean molecular mass of air M, the relative density profile $n_{\text{air}}(z)$, provided by the lidar return signal $P_{\text{off}}(z)$, can be integrated downward. This gives the relative pressure profile $p(z)$.

$$p(z) = p(z_0) + \int_z^{z_0} n_{\text{air}}(z) g(z) M dz \tag{5}$$

Division of relative pressure and density then yield the temperature profile $T(z)$. The downward integration requires an initial guess for $p(z_0)$ or $T(z_0)$ at the far range limit z_0 of the lidar return signal, usually around 80 km for the DWD lidar, above 90 km for the NASA lidar. Both algorithms use the CIRA 1986 climatology (Rees et al., 1990) to provide this initial guess. With decreasing altitude below the initialization altitude, the error made by assuming a climatological temperature or pressure decreases exponentially. At 10 km below initialization altitude, the error is typically less than 1 K, at 25 km below initialization altitude it is less than 0.1 K (e.g., Hauchecorne and Chanin, 1980; Steinbrecht, 1994).

As with ozone, the DWD and NASA temperature algorithms do some vertical smoothing on the lidar return signal $P_{\text{off}}(z)$ to reduce photon count noise. The DWD

algorithm uses a fixed 5 point (1.5 km) boxcar average at all altitudes. The NASA algorithm uses a variable width boxcar, with widths less than 3 km below 65 km, increasing to 6 km above 75 km. Figure 5 shows the widths of the running averages for the DWD and NASA algorithms. This width is a measure for the range resolution Δz of the retrieved temperature profiles. From Fig. 5 it is obvious, that temperature profiles retrieved by the DWD algorithm have the finer altitude resolution at most altitudes. However, combined with the DWD lidars much lower photon counts, this results in much noisier temperature data than from the NASA lidar.

3 Campaign overview

Two stable tropospheric high pressure systems provided excellent weather conditions during HOPE. The first system moved north-easterly, from Northern France to Scandinavia, over the period from 14 October to 20 October 2005. The second system was a long ridge moving from the Azores to the Baltic between 23 October and 1 November 2005. Both periods provided excellent clear nights for lidar measurements. Accordingly, the DWD and NASA-GSFC lidars were run simultaneously for 13 clear nights from 14 October to 31 October 2005. Both systems fired 50 laser pulses per second, synchronized to the chopper of the DWD system. This synchronization allowed both systems to acquire data simultaneously, without laser pulses from one system interfering with the other. For additional ozone profiles, seven Brewer/Mast ozonesondes were launched at Hohenpeissenberg. Daily temperature profiles came from the Vaisala RS92 radiosondes at the nearby station Munich (65 km north-east, near midnight, 00:00 UT), and from interpolation of 12:00 UT meteorological analyses by the US National Centers for Environmental Prediction (NCEP).

Figure 6 gives an overview of all ozone and temperature profiles during HOPE. The top panel shows the ozone profiles from the two lidar systems, and the Hohenpeissenberg ozonesondes. The bottom panel shows the temperature profiles. The lidars usually operated from one hour after sunset to one hour before sunrise, providing a

nightly mean profile centered around local midnight (23:00 UT). If clouds moved in during the night, the lidar measurement was terminated. It is then centered at an earlier time. Ozone- and radiosondes provide a snapshot only, which starts at launch-time at the ground, and ends about 90 min later at 30 to 35 km altitude. Four of the Hohenpeissenberg ozonesondes were launched at their usual early morning launch-time, after the lidar measurement. The other three ozonesondes were launched at night, to obtain better overlap with the lidars.

As expected for October, ozone number densities reached their maximum around 22 to 25 km altitude above sea level, at 3 to 4×10^{18} molecules per cubic meter. As usual, only small ozone variations were observed in the photochemically controlled altitudes above 25 km. Larger spatial and temporal variations were seen in the transport-controlled region below. Most of the time, ozone structures are reported in good agreement by all instruments, e.g. on 16 to 17 October 2005 near 21 km, or on October 27 to 28 October 2005 near 19 km. Sometimes, e.g. on 24 to 25 October 2005 near 18 km, the sonde reported a layer of low ozone not seen by the lidars. The two lidar systems show generally good agreement, with systematically higher ozone values reported by the NASA lidar around 35 to 40 km. Random ozone differences, with a slight tendency to higher values from the NASA lidar, are seen at altitudes near 18 to 22 km. There, the DWD lidar switches from the noisy near-range signal (acquired during the first and last hour of the night) to the far-range signal (acquired during the remainder of the night). The NASA lidar acquires near-range, far-range and Raman return signals simultaneously, throughout the night. By combining all these channels, ozone profiles from the NASA lidar reach further down, usually to 9 km. The DWD lidar reports ozone only down to about 15 km. In general, Fig. 6 shows good agreement between ozone from lidars and sondes.

The temperature profiles are summarized in the lower panel of Fig. 6. The regular Munich mid-night radiosondes, and the occasional Hohenpeissenberg ozonesondes cover the temperature profile from the ground up to 30 or 35 km. The DWD lidar gives temperature from 30 km up to 75 km. At altitudes below ≈28 km the DWD

lidar temperature measurement ends, because backscattering from the stratospheric aerosol layer begins to interfere. For the NASA lidar, the Raman channels are not affected much by aerosol, and allow temperature measurements down to 10 km. Due to its much more powerful return signal and coarser altitude resolution, the NASA lidar can measure temperature up to 90 km. The DWD lidar resolves finer temperature structures, but also shows higher noise. Both lidars show general agreement on the form of the temperature profiles and their major features. The large warming pulse near 65 km on 26 to 27 October 2005, for example, is reported by both lidars, as are the temperature minima and maxima near 60 and 66 km on 31 October/1 November. The DWD lidar reports the 26 to 27 October 2005 temperature peak already in the previous night near 70 km, whereas this earlier peak is not resolved well in the NASA temperature profile.

Both lidars tend to report slightly lower temperatures than the radiosondes in the 25 to 30 km region. Between 30 and 45 km, and during the first part of HOPE, the NCEP layer mean temperatures are also often higher than the lidar temperatures. The DWD lidar usually reports slightly lower temperatures than the NASA lidar in the 28 to 50 km region. As expected, since they use the same radiosonde type, temperatures agree very well between Munich and Hohenpeissenberg sondes. With the exception of temperature inversions near the ground, sondes and NCEP analyses agree very well too. This is also expected, because the analyses are based on assimilated radiosonde data.

4 Ozone and temperature differences

4.1 Individual nightly means

A more detailed picture of the ozone differences is given in Fig. 7. It shows the relative ozone difference between DWD and NASA lidar for all 13 nights. Before calculating difference profiles, all profiles were converted to a common 1 km altitude grid, by aver-

aging over the finer altitude bins available for the two lidars (and the sondes). Between 20 and 40 km, ozone differences between both lidars show low standard deviations, less than 10%. This is the altitude range where both systems give their most precise ozone measurements. From 23 to 33 km, ozone differences are very close to zero. From 34 to 39 km, all ozone differences are negative, indicating that the DWD lidar reports systematically lower ozone values than the NASA lidar. Near 20 km, there is also a tendency for negative differences, i.e. lower values from the DWD lidar. Above 42 km, the standard deviation of the ozone differences increases dramatically, from 7% at 40 km to more than 100% at 49 km. Above 50 km, the differences scatter widely, and the number of available comparisons drops from 12 at 49 km to 0 at 54 km, as the DWD lidar reaches its upper range limit for ozone. On the whole, Fig. 6 indicates fairly consistent ozone differences, less than 10% between 20 and 35 km, and reproducible to within 5% from 18 to 39 km.

The nightly mean temperature differences are given in Fig. 8. Between 30 and 60 km, differences are usually negative, indicating that the GSFC lidar gives around 2 K higher temperatures than the DWD lidar. From 30 to 50 km, temperature differences are reproducible to within 2 K. Above 55 km, standard deviation increases. Near 70 km, the DWD lidar reaches its upper range limit, and the number of available profiles drops rapidly.

4.2 Precision estimates

The standard deviation σ of the ozone and temperature differences in Figs. 7 and 8 can be used to check the precision estimates ΔX provided by the data processing algorithms for the two lidars. Largely, the precision of ozone and temperature profiles measured by a lidar is controlled by the statistical noise of the return signal photon counts (Hauchecorne and Chanin, 1980; Megie et al., 1985). If the first lidar estimates precision ΔX_1 for its nightly mean ozone or temperature profile X_1, and the second system estimates precision ΔX_2, the precision $\Delta_{\text{est}}(dX)$ for the difference pro-

file $dX = X_1 - X_2$ should be $\Delta_{est}(dX) = \left(\Delta X_1^2 + \Delta X_2^2\right)^{\frac{1}{2}}$. Photon count noise for the two systems should be uncorrelated, since both systems fire at different times, and count different photons.

If $\Delta_{est}(dX)$ is correct, it should be approximately the same as the standard deviation $\sigma_{meas}(dX)$, e.g. of the 13 nightly mean difference profiles during HOPE (blue line in Figs. 7 and 8). If the observed standard deviation $\sigma_{meas}(dX)$ differs substantially from the estimated precision $\Delta_{est}(dX)$, this indicates that either ΔX_1, or ΔX_2 (or both) are not correct. Note, however, that this check alone is not conclusive. Only gross errors in ΔX_i can be discovered. For example, ΔX_1 could be too low, ΔX_2 could be too high, but $\Delta_{est}(dX)$ could still come out correct.

Figures 9 and 10 show the precision estimates for ozone and temperature for the two lidars (ΔX_i, blue and green lines), and the precision estimate for the difference between the two lidars ($\Delta_{est}(dX)$, black lines). The red lines give the observed standard deviation $\sigma_{meas}(dX)$ of difference profiles during HOPE. For ozone, observed standard deviation and estimated precision behave similarly with altitude, with the best precision (lowest values) in the 20 to 40 km region. From 17 to 42 km, estimated precision and observed standard deviation are better (lower) than 10%. From 18 to 39 km, they are better than 5%. Below 28 km, the estimated ozone precision for the DWD lidar (blue line) is worse (larger values) than for the NASA lidar (green line). This is due to the weaker return signals (compare Fig. 2), and the shorter measurement time for the DWD near-range signals (below 22 km). Between 30 and 50 km, the estimated precision for the DWD lidar is slightly better than for the NASA lidar. At these altitudes, the much smaller photon counts of the DWD lidar are compensated by the much coarser altitude resolution of the DWD algorithm (compare Fig. 4).

Below 25 km, the agreement between observed standard deviation and estimated precision of the ozone differences is good. In this altitude region, the estimated precision of the difference (black line) is almost entirely controlled by the poor precision (large values) of the DWD lidar (blue line). The agreement between observed standard

deviation (red line) and estimated precision of the ozone differences (black line) below 25 km indicates that the ozone precision estimate from the DWD lidar is correct there.

From 27 to 48 km altitude, however, the estimated precision (black line) is better (smaller values) than the observed standard deviation (red line), by a factor of about 0.7. This indicates that the precision is under-estimated for at least one of the lidars. Comparison of ozone standard deviation and estimated precision for the DWD lidar over many years (not shown) indicates that the precision estimate for this lidar is correct above 45 km, where the observed standard deviation is dominated by statistical noise. For the NASA lidar during HOPE, however, the standard deviation between 45 and 50 km (not shown) is larger than for the DWD lidar, by a factor of about 1.7, although the estimated precisions are comparable. Multiplying the NASA ozone precision estimate (ΔX, green line) by a factor of 1.7 would also increase the estimate for the precision of DWD-NASA ozone differences ($\Delta_{\text{est}}(dX)$, black line) between 25 and 50 km. This would bring it into good agreement with the observed standard deviation ($\sigma_{\text{meas}}(dX)$, red line) at all altitudes. From Fig. 9, and some additional information, it appears that the ozone precision values given by the NASA algorithm are currently too small by a factor of about 1.7.

For temperature in Fig. 10, the observed standard deviation of DWD-NASA temperature differences ($\sigma_{\text{meas}}(dX)$, red curve), as well as the precision estimate ($\Delta_{\text{est}}(dX)$, black curve) increase with altitude, from 0.4 K around 30 km to more than 10 K above 70 km. Different from ozone, the estimated precision for temperature differences (black curve) is much larger than the observed standard deviation (red curve). Figure 10 shows that the precision is over-estimated (values too large) by a factor of about 2. Since the black curve is almost entirely controlled by the estimated emperature precision from the DWD lidar (ΔX, blue line), the disagreement between the black and red curves points to an error in the DWD temperature precision estimate. In fact, the current DWD processing does not account for the noise reduction obtained by averaging over 5 range bins (see discussion of Fig. 5). This should reduce statistical noise by a factor of $\sqrt{5}\approx 2.2$, roughly the same factor that would bring the black and red curves in

AMTD
2, 37–86, 2009

Fig. 10 into agreement. Temperature precision for the NASA lidar (ΔX, green curve) is estimated to be between 0.4 K and 1 K. This is much better than for the DWD lidar, and is due to the much higher return signals and the coarser altitude resolution for the NASA lidar. Since the estimated temperature precision for the NASA lidar is so much better (smaller), Fig. 10 does not provide much information about correctness of the NASA precision estimate for temperature.

4.3 Average ozone differences

We now return to the topic of systematic differences between the different instruments. Figure 11 shows the average relative ozone difference between DWD and NASA lidar during HOPE (blue line). The blue line in Fig. 11 is the average of the 13 individual difference profiles given in Fig. 7. Systematic ozone differences seen previously for the DWD lidar against the SAGE II and GOMOS satellite instruments (Steinbrecht et al., 2006; Meijer et al., 2004) are plotted as well (black and green lines). All profiles look very similar. Error bars overlap at nearly all altitudes. In all comparisons, the DWD lidar profiles have a clear negative bias between 33 and 43 km, by up to 15% near 39 km. Between 23 and 33 km, the DWD profiles agree within 2% with NASA lidar and SAGE II. GOMOS seems to have a high bias, but error bars are larger as well.

Near 20 km and below, the DWD lidar gives up to 7% lower ozone values than the NASA lidar (blue curve). A similar difference is seen against SAGE II and GOMOS (black and green curves). Lower ozone values are also reported by the ozonesondes below 20 km (red line), but the sondes are consistent with the DWD lidar there. The sondes also show a low bias above 30 km. The latter bias is well known and is attributed to an insufficient correction of decreasing pump efficiency at low ambient pressure (Steinbrecht et al., 1998, WMO correction is still used).

Figure 12 addresses the question, why the DWD lidar consistently underestimates ozone in the 33 to 43 km region. The figure compares the systematic difference observed during HOPE (blue line), with differences generated by the DWD ozone processing algorithm. The DWD algorithm has been tested previously with synthetic sim-

ulated lidar return signals in the NDSC algorithm intercomparison (Godin et al., 1999, red line). There, the DWD ozone algorithm showed a bias very similar to the ozone difference found in HOPE. A slight shift towards lower altitudes comes from the different ozone profile used in this NDSC algorithm intercomparison. For HOPE, return signals from the NASA lidar were also processed with the DWD algorithm. The black line gives the resulting DWD-NASA ozone difference. As in the Godin et al. (1999) NDSC algorithm intercomparison, this difference comes from the processing algorithm, more specifically from the differential filters used in the DWD and NASA algorithm (compare Fig. 3). For HOPE, the difference caused by the DWD algorithm is virtually the same as the observed ozone difference (blue line). From the good agreement between observed ozone difference during HOPE and the bias found for the DWD algorithm in Fig. 12, it becomes clear that the bias of the DWD lidar ozone profiles against several other instruments in the 33 to 43 km region is caused by the DWD processing algorithm, not by the lidar hardware.

4.4 Average temperature differences

The average temperature difference profiles are given in Fig. 13. Temperatures from DWD lidar, NCEP operational analyses, and from Munich radiosondes are referenced to the NASA lidar temperature. From 25 km to 65 km, the DWD lidar measures on average 1 to 2 K lower temperature than the NASA lidar. This difference is statistically significant from 25 to 50 km. Above 65 km, the DWD lidar reports up 15 K higher temperature than the NASA lidar, but this is not statistically significant. The NASA lidar itself reports about 1 K lower temperatures than NCEP at most altitudes. This is statistically significant between 16 and 36 km. NASA lidar temperatures are also between 0.2 and 1.2 K lower than temperature measured by the Munich radiosondes between 15 and 33 km. This is often not statistically significant, but in agreement with the NCEP temperatures. All differences seem to be fairly constant over a wide altitude range. From Fig. 13 it appears that

1. NCEP analyses provide very similar temperatures to the radiosondes, which are of course an important input to the analyses.

2. The NASA lidar reports about 1 K lower temperature than analyses or radiosondes.

3. The DWD lidar reports 1 to 2 K lower temperature than the NASA lidar, and 2 to 4 K lower temperature than NCEP analyses or radiosondes.

To put the HOPE temperature differences into a wider context, Fig. 14 compares them with long-term average temperature differences between NCEP and DWD lidar, and between Hohenpeissenberg soundings and DWD lidar. Note that Fig. 14 uses the DWD lidar as the reference. The temperature differences during HOPE (orange, magenta and blue line) are fully consistent with the differences found previously, when comparing DWD lidar temperatures with NCEP over the period 2001 to 2007, or with radiosondes over the period 1997 to 2007 (green and red lines). At all altitudes between 25 and 65 km, the DWD lidar consistently reports between 1 and 4 K lower temperature. Systematic differences between RS80 and RS92 radiosondes (Steinbrecht et al., 2008) are minor in this context. Section 5 explains later, where this large temperature difference comes from.

4.5 Correlation and scatter plots

It is of course desirable that all instruments (and the NCEP analyses) should provide the same mean profiles of ozone and temperature. In addition, variations should also be tracked in the same way by all instruments. A climatology, for example, might give the correct mean profile, but it would probably not provide correct variations. To address this important aspect, Fig. 15 plots ozone variations measured by DWD lidar and ozonesondes against ozone from the NASA lidar, at different altitude levels. Ideally, all data points in each panel would lie on the 1 to 1 line, from bottom left to top right.

As expected, the lowest scatter and the tightest correlations are seen between 25

and 40 km altitude, the altitude range of best precision for the lidars. Both lidars report a similar range of ozone values, and highly correlated variations (correlation $R>0.9$). However, because of the systematic underestimation by the DWD algorithm (see Figs. 11 and 12), most blue data points at 35 and 40 km altitude fall below the 1 to 1 line. As noise increases with altitude above 40 km, data points scatter more widely and lie more or less randomly around the 1 to 1 line. At 15 and 20 km, the larger spatial and temporal variability of ozone (compare Fig. 6), and the poorer precision of the DWD lidar (compare Fig. 9), also result in increased scatter. Ozonesonde precision is around 5% (e.g., Smit and Kley, 1998), and the scatter of the ozonesonde data in Fig. 15 is comparable to the lidar results. Even the two sondes with poor temporal matches (circled triangles in Fig. 15; 12 October 2005, more than 60 h before a lidar measurement, 24 October 2005, 12 h before a lidar measurement), give data in the range of the other sondes, launched within 2 to 6 h of the lidar measurement.

Figure 16 gives the vertical profile of the correlation coefficient between ozone variations from the different instruments during HOPE. Ozone measured by the DWD lidar correlates slightly better with NASA ozone than with ozone from the sondes. The confidence interval is also narrower. For the DWD lidar, correlation with NASA ozone is significantly larger than zero at most altitudes between 15 and 42 km. Between 25 and 37 km, ozone correlation between the two lidars is better than 0.9. From 40 to 50 km measurement noise increases substantially. The correlation drops from 0.8 to near zero. Below 25 km, correlations range between 0.5 and 0.9, and are similar for DWD lidar and ozonesondes. The poor correlation around 22 km, near the ozone maximum, is attributed to small-scale structures that vary with time and location and are sampled differently by the sondes and the two lidars (compare Fig. 6).

Figures 17 and 18 plot the temperatures recorded by the other instruments during HOPE against temperature from the NASA lidar. From 30 to 42 km, all data sources show very similar variations. Data points lie close to the ideal 1 to 1 line, with an apparent warm bias for NCEP analyses and radiosondes, and an apparent cold bias for the DWD lidar (compare Fig. 13). At higher altitudes (48 to 70 km), data points scatter

more widely, as the measurements become increasingly noisy. The two top-most layers of the NCEP analyses (48 and 53 km, or 1 and 0.4 hPa) show little correlation with temperature from the NASA lidar (or the DWD lidar). Temperature correlation between the two lidars is generally better, and appears to be useful up to 70 km.

For the lower levels (Fig. 18), data points from radiosondes and NCEP are very similar, and are generally close to the 1 to 1 line. Radiosonde and NCEP temperatures correlate well with the NASA lidar results. Vertical profiles of the correlations are given in Fig. 19. With the exception of the NCEP data around 14 km, correlations with the NASA lidar data are larger than 0.8 for all data sets at all levels up to 37 km. Closer inspection in Fig. 6 indicates that the large scale NCEP data do not resolve local details of the tropopause near 14 km. Usually, however, correlation between lidar and NCEP temperatures is slightly higher than between lidar and the sondes. Figure 6 indicates that the sondes report local short-term structures not present in the nightly mean lidar profiles and smooth NCEP profiles. Above 50 km, correlation between the two lidars decreases, because noise increases and the precision of the lidar temperature measurements drops, especially for the DWD lidar (see Fig. 9). Nevertheless, significant correlation appears up to 70 km.

5 Errors affecting the DWD lidar data

When trying to explain the consistent low bias of the DWD lidar temperature data, e.g. in Fig. 13, a major advantage of the HOPE intercomparison was to have the directly comparable return signals $P(z)$ from the GSFC lidar. In the end, analysis of the return signals from both lidars indicated a systematic error in the assigned altitude z for the DWD lidar return signals. The ratio $P_{\mathrm{DWD}}(z)/P_{\mathrm{GSFC}}(z)$, which should be constant with altitude, and the reported altitude of cirrus clouds showed that the assigned altitudes of the DWD lidar are too high by about 300 m during HOPE. Detailed tests with the DWD lidar confirmed this. The “laser-synch” trigger pulse, which starts the range measurement of the DWD lidar, comes $1.9\pm0.3\,\mu$s, or 290 ± 45 m, earlier than the actual optical

pulse. Therefore, all altitudes reported by the DWD lidar are too high by about 290 m, and need to be shifted downwards. Very likely this has been the case throughout the entire DWD lidar record since 1987.

This altitude offset has a slightly different effect on ozone and temperature profiles:

- Ozone profiles simply have to be shifted in altitude. For the Δz=+290 m altitude error found for the DWD lidar, all ozone profiles are too high by 290 m. The ozone error for unshifted profiles is inversely proportional to the ozone vertical gradient. The error is zero near the ozone maximum at 23 km. It is negative at altitudes below the ozone maximum (low ozone shifted up), up to −10% near 15 km. It is positive above the ozone maximum (high ozone shifted up), up to +11% near 47 km.

- Temperature profiles are also shifted in altitude. In addition, however, the underlying density estimate, $n_{\mathrm{air}}(z) \propto P(z)\, z^2$, is too high because the assigned z is too large. Too large density then results in too low temperature. Near 40 km, the density error is $(40.29/40)^2 - 1$, about 1.4%. The vertical shift effect is about 1 K (colder temperatures shifted up). Both effects combine to make the temperature estimate from the DWD lidar too cold, as seen in Figs. 13 and 14.

In addition, it turned out that the DWD temperature algorithm uses slightly too low values for $g(z)$, the acceleration due to Earth's gravity. 9.793 ms^{-2} were used for $g(0)$, instead of 9.809 ms^{-2}, the correct value at 48° N (e.g., WGS, 2000, Eq. 4-1). This affects the hydrostatic equilibrium pressure calculation, and therefore the retrieved temperature. By itself, the low $g(z)$ also results in too low temperatures for the DWD lidar. The net effect of all errors is a nearly constant offset for the temperature profiles, and a small altitude shift for the ozone profiles. The scatter diagrams in Sect. 4.5, as well as the standard deviations and error estimates in Sect. 4.2 are affected very little by these errors. They remain valid.

However, the average differences between DWD lidar ozone and temperature profiles in Figs. 11 to 14 change substantially when the above errors are corrected. Fig-

AMTD
2, 37–86, 2009

ures 20 and 21 repeat the uncorrected HOPE average ozone and temperature differences from before (blue lines), and compare them with corrected DWD lidar results (violet lines).

For ozone in Fig. 20, only the downward shift has to be considered. It results in better agreement with the GSFC lidar between 16 and 25 km. The corrected DWD lidar ozone profiles (violet line) show no significant difference to the NASA profiles over this altitude range. At these altitudes, agreement with SAGE and GOMOS would also improve (compare Fig. 11). The corrected profile difference (violet line) also agrees better with the difference expected from the algorithm (black line in Figs. 12 or 20). Between 25 and 32 km, using the corrected altitudes changes the difference to the GSFC lidar from small positive values to small negative values. Above 33 km, differences become larger. As before, differences cease to be significant above about 44 km. Between 30 to 40 km, much of the difference can be attributed to the systematic bias of the DWD algorithm, as mentioned several times.

For temperature, altitude shift and corrected $g(z)$ have to be considered. When this is done, agreement of DWD lidar temperatures with the GSFC data improves significantly, as shown by the violet line in Fig. 21. DWD temperatures increase by 1 to 2 K between 30 and 50 km. Except for near 45 km altitude, the corrected DWD temperatures now show no significant difference to the GSFC data. The corrected DWD lidar temperatures also come into better agreement with sonde and NDSC temperatures (compare Figs. 13 and 14).

The detailed analysis made possible by the collocation of two lidar systems during HOPE has uncovered two long-standing errors in the DWD data processing: The 290 m range shift, and the low values for $g(z)$. When corrected, much of the systematic temperature difference, that has been seen also in previous intercomparisons, is removed. The effect on the ozone profiles is also important, but less obvious. It is again consistent with previous intercomparisons, e.g. against SAGE or GOMOS. From the available information, it seems that the altitude shift has been present in the DWD lidar data from the beginning in 1987. While this means that it took 20 years to uncover

the problem, it also means that the time series is still internally consistent. Ozone and temperature changes observed by the DWD lidar over the years (e.g. Steinbrecht et al., 2006) remain valid!

6 Conclusions

Thirteen clear nights in October 2005 have allowed the successful intercomparison of the DWD ozone and temperature lidar at Hohenpeissenberg with the NDACC travelling standard lidar operated by NASA's Goddard Space Flight Center. Additional comparison profiles were provided by Brewer/Mast ozonesondes started at Hohenpeissenberg, by Vaisala RS92 radiosondes launched at Munich (65 km to the north-east), and by operational NCEP analyses.

The HOPE intercomparison confirmed a low bias for ozone profiles from the DWD lidar in the 33 to 43 km region, by up to 10%. This bias has been seen in previous intercomparisons, e.g. against SAGE, GOMOS or GOME. It is caused by the DWD ozone processing algorithm. At most altitudes between 20 and 33 km, however, systematic ozone differences of DWD lidar or ozonesondes against the NASA lidar are smaller than 3 to 5%. Below 20 km, the DWD lidar reports up to 7% lower ozone than the NASA lidar or SAGE and GOMOS. Detailed analysis, made possible by the HOPE intercomparison, indicates that this bias is caused by an erroneous upward shift of the DWD lidar data by 290 m. This altitude shift needs to be corrected in a future reprocessing.

Like previous campaigns, HOPE has demonstrated that lidars deliver their best precision, better than 5%, for ozone between 20 and 40 km altitude. Above 45 km, lidar ozone data become increasingly noisy. Precision drops from around 10% near 45 km to 50% or worse near 50 km. The DWD lidar compensates for its much weaker return signals by using a much coarser range resolution. Ozone variations from the two lidars track very well. Correlations are higher than 0.8 at most altitudes from 15 to 40 km. As the ozone data become increasingly noisy above 40 km, correlations drop to zero

around 50 km. Up to 30 km, the ozonesondes also provide good measurements, with virtually no bias between 20 and 30 km, and a low bias up to 5% above 30 km. Precision of the ozonesondes is 5 to 10%. Correlation between ozonesondes and lidar is in the range 0.6 to 0.9, not quite as good as between the two lidars. In part, this might reflect the different character of the very local in-situ measurement by the sondes and the nightly mean profiles from the lidars.

Temperature data from the DWD lidar have a 1 to 2 K cold bias over the entire region from 30 to 65 km against profiles from the NASA lidar, and a 2 to 4 K cold bias against Vaisala RS92 radiosondes or NCEP analyses. As with ozone, the temperature bias during HOPE is consistent with multi-year intercomparisons between DWD lidar and NCEP analyses or radiosondes. The altitude shift and slightly too low $g(z)$ discovered by the detailed analysis of the HOPE data can now finally explain most of this long-standing bias. Interestingly, both lidars report slightly lower temperatures than radiosondes or NCEP analyses, by around 1 K between 15 and 50 km.

For temperature, precision of the DWD lidar is better than 2 K in the 30 to 50 km altitude range, decreasing to 10 K near 70 km. The HOPE comparison has shown that the current DWD algorithm over-estimates temperature precision, because ist does not account for the noise reduction obtained by averaging over 5 range bins. Estimated temperature precision values should be reduced by a factor $\sqrt{5}\approx 2.2$ (e.g. from 22 K to 10 K, near 70 km). The NASA lidar uses a much coarser altitude resolution for temperature and estimates precision better than 1 K between 20 and 75 km. This is very precise and could not be checked with the data available in HOPE. Between 10 and 40 km, temperature variations are tracked very similarly by both lidars, Munich radiosondes, and NCEP analyses. Correlation coefficients are usually larger than 0.8 to 0.9. Above 40 km, temperatures from the three topmost levels of the NCEP analyses do not track the lidar results well (R approaches zero), whereas the two lidars show reasonable tracking ($R>0.4$) up to 70 km.

The ozone and temperature biases confirmed by the HOPE intercomparison have been present in the DWD lidar record since the beginning in 1987. Long-term com-

parison with ozone records from SAGE and HALOE indicates no change over time for the ozone bias (Steinbrecht et al., 2006). Comparison of the temperature record with NCEP and ECWMF re-analyses (unpublished results) indicates good long-term stability for temperature as well. To our present knowledge, the Hohenpeissenberg lidar record for ozone and temperature is internally consistent. It is suited for long-term trend analysis. HOPE has been instrumental for discovering and defining several errors, that have been present for a long time. It is now necessary to fix and improve the DWD ozone and temperature algorithms. Then, the entire data set since 1987 needs to be re-processed and re-submitted to NDACC and other relevant data centers.

Acknowledgements. We thank S. Steiner and M. Adelwart, who carefully prepared the ozone sondes, and launched them very successfully at various times early in the morning and late at night. F. Riesemann helped to sort out odds and ends during the campaign. The Hohenpeissenberg group thanks P. Newman and M. Heney for providing NCEP temperature data over many years on a daily basis.

References

Braathen, G. O., Godin-Beekmann, S., Keckhut, P., McGee, T. J., Gross, M. R., Vialle, C., and Hauchecorne, A.: Intercomparison of stratospheric ozone and temperature measurements at the Observatoire de Haute Provence during the OTOIC NDSC validation campaign from 118 July 1997, Atmos. Chem. Phys. Discuss., 4, 5303–5344, 2004, http://www.atmos-chem-phys-discuss.net/4/5303/2004/. 39

Brinksma, E. J., Meijer, Y., McDermid, I. S., Cageao, R., Bergwerff, J., Swart, D. P. J., Ubachs, W., Matthews, A., Hogervorst, W., and Hovenier, J.: First lidar observations of mesospheric hydroxyl, Geophys. Res. Lett., 25, 51-54, 1998. 67

Claude, H., Schönenborn, F., Steinbrecht, W., and Vandersee, W.: New evidence for ozone depletion in the upper stratosphere, Geophys. Res. Lett., 21(22), 2409–2412, 1994. 40

Carswell, A. I., Pal, S. R., Steinbrecht, W., Whiteway, J. A., Ulitsky, A., and Wang, T. Y.: Lidar measurements of the middle atmosphere Can. J. Phys., 69, 1076–1086, 1991. 39, 42

Ferrare, R. A., McGee, T. J., Whiteman, D., Burris, J., Owens, M., Butler, J., Barnes, R. A., Schmidlin, F., Komhyr, W., Wang, P. H., McCormick, M. P., and Miller, A. J.: Lidar measure-

ments of stratospheric temperature during STOIC, J. Geophys. Res., 100(D5), 9303–9312, 1995.

Geh, B.: Aufbau einer automatischen Apparatur zur Messung der stratosphärischen Ozonkonzentration, Diploma thesis, Ludwig-Maximilians Universität, Munich, 66 pp., 1987. 40, 41

Godin, S., Carswell, A. I., Donovan, D. P., Claude, H., Steinbrecht, W., McDermid, I. S., McGee, T. J., Gross, M. R., Nakane, H., Swart, D. P. J., Bergwerff, H. B., and Uchino, O.: Ozone Differential Absorption Lidar Algorithm Intercomparison, Appl. Opt., 38, 6225–6236, 1999. 43, 52, 77

Gross, M. R., McGee, T. J., Ferrare, R. A., Singh, U., and Kimvilikani, P.: Temperature Measurements Made with a Combined Rayleigh-Mie/Raman Lidar, Appl. Opt., 24, 5987-5995, 1997. 40

Hauchecorne, A. and Chanin, M.-L.: Density and temperature profiles obtained by lidar between 35 and 70 km, Geophys. Res. Lett., 7, 565-568, 1980. 39, 44, 48

Iikura, Y., Sugimoto, N., Sasano, Y., and Shimzu, H.: Improvement on lidar data processing for stratospheric aerosol measurements, Appl. Opt., 26, 5299-5306, 1987. 41

Keckhut, P., McDermid, I. S., Swart, D. P. J., McGee, T., Godin-Beekmann, S., Adriani, A., Barnes, J., Baray, J.-L., Bencherif, H., Claude, H., di Sarra, A.G., Fiocco, G., Hansen, G., Hauchecorne, A., Leblanc, T., Lee, C.H., Pal, S., Megie, G., Nakane, H., Neuber, R., Steinbrecht, W., and Thayer, J.: Review of ozone and temperature lidar validations performed within the framework of the Network for the Detection of Stratospheric Change, J. Environ. Monit., 6, 1-14, 2004. 39

Margitan, J. J., Barnes, R. A., Brothers, G. B., Butler, J., Burris, J., Connor, B. J., Ferrare, R. A., Kerr, J. B., Komhyr, W. D., McCormick, M. P., McDermid, I. S., McElroy, C. T., McGee, T. J., Miller, A. J., Owens, M., Parrish, A. D., Parsons, C. L., Torres, A. L., Tsou, J. J., Walsh, T. D., and Whiteman, D.: Stratospheric ozone intercomparison campaign (STOIC) 1989: Overview, J. Geophys. Res., 100(D5), 9193–9208, 1995. 39

McDermid, I. S., Bergwerff, J., Bodeker, G. E., Boyd, I., Brinksma, E., Connor, B., Farmer, R., Gross, M., Kimvilakani, P., Matthews, W., McGee, T., Ormel, F., Parrish, A., Singh, U., Swart, D., Tsou, J., Wang, P., and Zawodny, J.: OPAL: Network for the Detection of Stratospheric Change Ozone Profiler Assessment at Lauder, New Zealand 1. Blind intercomparison, J. Geophys. Res., 103(D22), 28683–28692, 1998a. 39

McDermid, I. S., Bergwerff, J., Bodeker, G. E., Boyd, I., Brinksma, E., Connor, B., Farmer, R.,

Gross, M., Kimvilakani, P., Matthews, W., McGee, T., Ormel, F., Parrish, A., Singh, U., Swart, D., and Tsou, J.: OPAL: Network for the detection of stratospheric change ozone profiler assessment at Lauder, New Zealand 2. Intercomparison of revised results, J. Geophys. Res., 103(D22), 28693–28700, 1998b.

McGee, T. J., Whiteman, D., Ferrare, R., Butler, J. J., and Burris, J.: STROZ LITE: Stratospheric Ozone Lidar Trailer Experiment, Opt. Eng., 30, 31-39, 1991. 40

McGee, T. J., Gross, M. R., Ferrare, R., Heaps, W., and Singh, U. N.: Raman DIAL measurements of stratospheric ozone in the presence of volcanic aerosols, Geophys. Res. Lett., 20, 955-958, 1993. 40

McGee, T. J., Gross, M. R., Singh, U. N., Butler, J. J., and Kimvilakani, P. E.: Improved stratospheric ozone lidar, Opt. Eng., 34, 1421-1430, 1995a. 40, 41

McGee, T. J., Ferrare, R. A., Whiteman, D., Butler, J. J., Burris, J. F., and Owens, M. A.: Lidar measurements of stratospheric ozone during the STOIC campaign, J. Geophys. Res., 100(D5), 9255–9262, 1995b.

McGee, T. J., Gross, M. R., Singh, U. N., Kimvilakani, P., Matthews, A., Bodeker, G., Connor, B., Tsou, J. J., Proffitt, M., and Margitan, J.: Vertical profile measurements of ozone at Lauder, New Zealand during ASHOE/MAESA, J. Geophys. Res., 102(D11), 13283–13290, 1997.

McPeters, R. D., Hofmann, D., Clark, M., Flynn, L., Froidevaux, L., Gross, M., Johnson, B., Koenig, G., Liu, X., McDermid, I. S., McGee, T., Murcray, F., Newchurch, M.J., Oltmans, S., Parrish, A., Schnell, R., Singh, U., Tsou, J. J., Walsh, T., and Zawodny, J. M.: Results from the 1995 stratospheric ozone profile intercomparison at Mauna Loa, J. Geophys. Res., 104(D23), 30505-30514, 1999.

Meijer, Y. J., Swart, D. P. J., Allaart, M., Andersen, S. B., Bodeker, G., Boyd, I., Braathen, G., Calisesi, Y., Claude, H., Dorokhov, V., von der Gathen, P., Gil, M., Godin-Beekmann, S., Goutail, F., Hansen, G., Karpetchko, A., Keckhut, P., Kelder, H. M., Koelemeijer, R., Kois, B., Koopman, R. M., Kopp, G., Lambert, J.-C., Leblanc, T., McDermid, I. S., Pal, S., Schets, H., Stubi, R., Suortti, T., Visconti, G., and Yela, M.: Pole-to-pole validation of Envisat GOMOS ozone profiles using data from ground-based and balloon sonde measurements, J. Geophys. Res., 109, D23305, doi:10.1029/2004JD004834, 2004. 51, 76

Megie, G. J., Ancellet, G., and Pelon, J.: Lidar measurements of ozone vertical profiles, Appl. Opt., 24, 3454–3463, 1985. 39, 42, 48

Press, W. H., Teukolsky, S. A., Vetterling W. T., and Flannery B. P.: Numerical Recipes in C, Cambridge University Press, Cambridge, UK, 994 pp., 1992. 43

Rees, D., Barnett, J. J., and Labitzke, K. (Eds.): COSPAR International reference atmosphere: 1986 Part II: Middle Atmosphere Models, Pergamon Press, Oxford, UK, 519 pp., 1990. 44

Smit, H. G. J and Kley, D.: JOSIE: The 1996 WMO International intercomparison of ozonesondes under quasi flight conditions in the environmental simulation chamber at Jülich, WMO GAW report No. 130, WMO-TD No. 926, World Meteorological Organization, Geneva, 108 pp., 1998 (available from http://www.fz-juelich.de/icg/icg-2/josie/1996/). 54

Steinbrecht, W., Rothe, K. W., and Walther, H.: Lidar setup for daytime and nighttime probing of stratospheric ozone and measurements in polar and equatorial regions, Appl. Opt., 28, 3616–3624, 1989. 41

Steinbrecht, W.: Lidar measurements of ozone, aerosol, and temperature, PhD thesis, York University, Toronto, Canada, 250 pp., 1994. 44

Steinbrecht, W. and Carswell, A. I.: Evaluation of the effects of Mount Pinatubo aerosol on differential absorption lidar measurements of stratospheric ozone, J. Geophys. Res., 100(D1), 1215–1234, 1995. 42

Steinbrecht, W., Winkler, P., and Claude, H.: Ozon- und Temperaturmessungen mittels Lidar am Hohenpeissenberg. Rep. No. 200, Deutscher Wetterdienst, Offenbach, 89 pp., 1997. 40, 43

Steinbrecht, W., Schwarz, R., and Claude, H.: New Pump Correction for the Brewer-Mast Ozone Sonde: Determination from Experiment and Instrument Intercomparisons, J. Atmos. Ocean. Tech. 15, 144–156, 1998. 51

Steinbrecht W., Claude, H., Schönenborn, F., McDermid, I.S., Leblanc, T., Godin, S., Song, T., Swart, D. P. J., Meijer, Y. J., Bodeker, G. E., Connor, J., Kämpfer, N., Hocke, K., Calisesi, Y., Schneider, N., de la Noë, J., Parrish, A. D., Boyd, I. S., Brühl, C., Steil, B., Giorgetta, M. A., Manzini, E., Thomason, L. W., Zawodny, J. M., McCormick, M. P., Russell III, J. M., Bhartia, P. K., Stolarski, R. S., and Hollandsworth-Frith, S. M.: Long-term evolution of upper stratospheric ozone at selected stations of the Network for the Detection of Stratospheric Change (NDSC), J. Geophys. Res., 111, D10308, doi:10.1029/2005JD006454, 2006. 40, 51, 58, 60, 76

Steinbrecht W., Claude, H., Schönenborn, F., Leiterer, U., Dier, H., and Lanzinger, E.: Pressure and Temperature Differences between Vaisala RS80 and RS92 Radiosonde-Systems J. Atmos. Ocean. Tech., 25, 909–927, doi:10.1175/2007JTECHA999.1, 2008. 53

Werner J., Rothe, K. W., and Walther, H.: Monitoring of the stratospheric ozone layer by laser radar, Appl. Phys., B 32, 113–118, 1983. 41

Williamson, C. K. and De Young, R. J.: Method for the reduction of signal-induced noise in photomultiplier tubes, Appl. Opt., 39, 1973–1979, 2000. 41

WGS84: Department of Defense World Geodetic System 1984, Report 8350.2, 3rd edition, US National Imagery and Mapping Agency, Bethesda, Maryland, 175 pp., available at: http://earth-info.nga.mil/GandG/wgs84/, 2000. 56

Table 1. Main characteristics of the NASA Goddard Space Flight Center Stratospheric Ozone Lidar in Trailer Experiment (308 and 355 nm channels only), and of the DWD ozone lidar at Hohenpeissenberg.

	NASA	DWD
Transmitter		
$\lambda_{on}/\lambda_{off}$	308/355 nm	308/353 nm
Laser @λ_{on}	Lambda Physik LPX 320	Lambda Physik LPX 220i
Light source @λ_{off}	Spectra Physics Quanta Ray PIV-400 Nd:YAG×3	H_2 Raman Cell
transmitted pulse energy @$\lambda_{on}/\lambda_{off}$	300 mJ/150 mJ	100 mJ/10 mJ
Receiver Telescope		
telescope setup	Dall-Kirkham	Newtonian
mirror diameter	0.76 m	0.6 m
field of view	2.3 mrad	0.4 mrad
focal length	3.66 m	2.4 m
receiver channels	308 nm (HI + LOW), 355 nm (HI + LOW) 332 nm, 387 nm (HI+LOW), 407 nm	308 and 353 nm
Interference Filters		
manufacturer	Barr Associates	Barr Associates
peak transmission @$\lambda_{on}/\lambda_{off}$	73/52%	50/65% (before 11/98 30/25%)
width (FWHM) @$\lambda_{on}/\lambda_{off}$	1.1/0.92 nm	5/2 nm (before October 1998: 10/2.5 nm)
Photon Counting		
photomultipliers	Hamamatsu 7400 P-03	EMI 9893QA/350
maximum used count rate @$\lambda_{on}/\lambda_{off}$	10/40 MHz	6/2 MHz
signal induced noise @$\lambda_{on}/\lambda_{off}$ (near 100 km)		<3 Hz/< 0.3 Hz
HV range gating	all channels	– none –
bowtie chopper	308 nm HI channel	both channels
multichannel scalers	LICEL 300 MHz	Optech FDC 700 (before February 1995: LeCroy 3521)

AMTD
2, 37–86, 2009

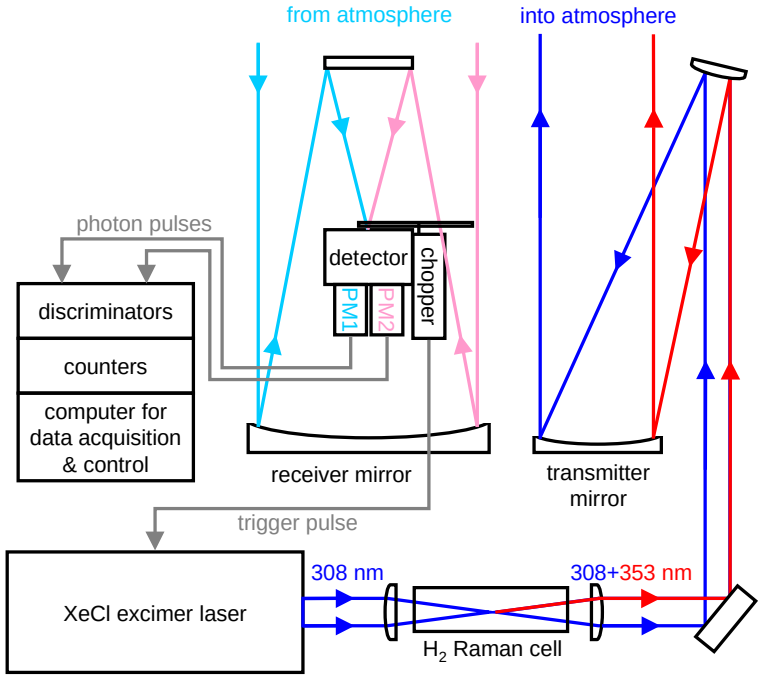

Fig. 1. Schematic of the DWD lidar system at Hohenpeissenberg (47.8° N, 11.0° E, 976 m a.s.l.). PM1, PM2 = photomultipliers for 308 and 353 nm.

AMTD
2, 37–86, 2009

HOPE 2005

W. Steinbrecht et al.

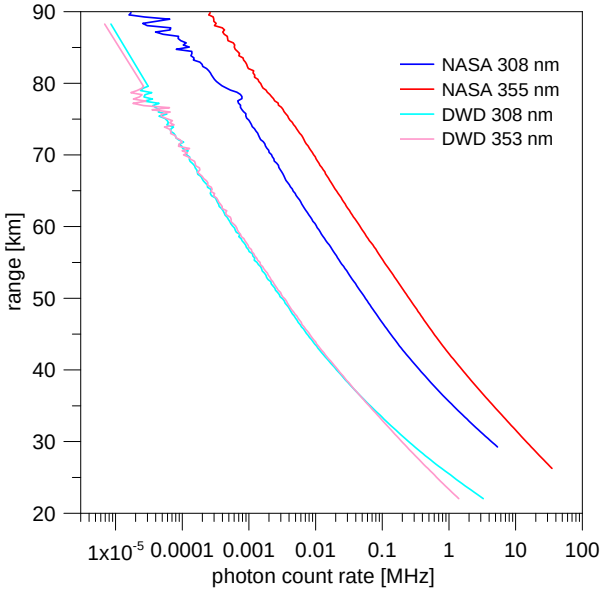

Fig. 2. Average return signals for NASA and DWD lidar for the night of 27 to 28 October 2005, from 18:18 to 03:59 UT, and from 19:25 to 04:21 UT, respectively. Only the high-range signals are shown. NASA lidar uses 15 m range bins, which are summed here to give 300 m range bins. The DWD lidar uses 300 m range bins below 80 km, and 17 km bins above 80 km, to reduce photon count noise. The peak in the NASA 308 nm return signal near 78 km is caused by resonance scattering from the mesospheric OH-layer (Brinksma et al., 1998). The different slopes of the blue and red lines between 20 and 35 km are due to ozone absorption.

AMTD
2, 37–86, 2009

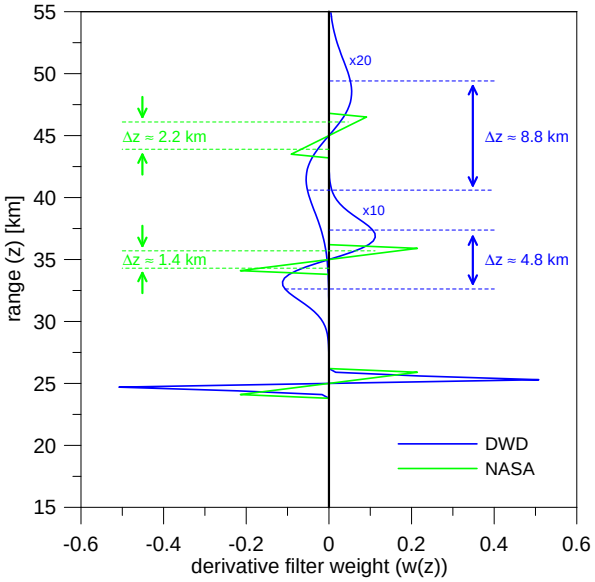

Fig. 3. Derivative filter weights $w(i)$ for DWD (blue line) and NASA (green line) ozone processing algorithms at 25, 35 and 45 km altitude (above the lidar). For clarity, the DWD filter weights at 35 and 45 km have been multiplied by 10 and 20. At 35 and 45 km, the distance between the dashed lines gives the effective width Δz of the filters, as defined in Eq. 3. The effective width at 25 km is not shown, but is 0.8 km and 1.4 km for DWD and NASA processing, respectively.

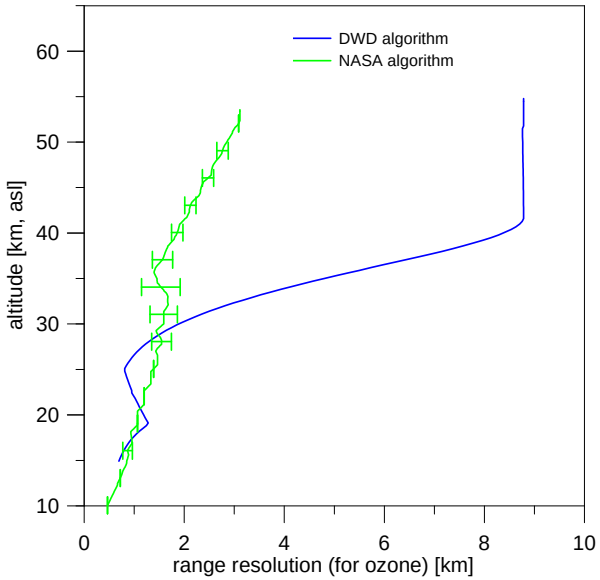

Fig. 4. Range resolution Δz of the derivative filters $w(z)$ for NASA and DWD ozone processing algorithms. NASA adapts the range resolution individually to the return signals of each night. Therefore, standard deviation (1σ error bars) and average range resolution are plotted for the NASA algorithm. The DWD range resolution is the same for every night.

AMTD
2, 37–86, 2009

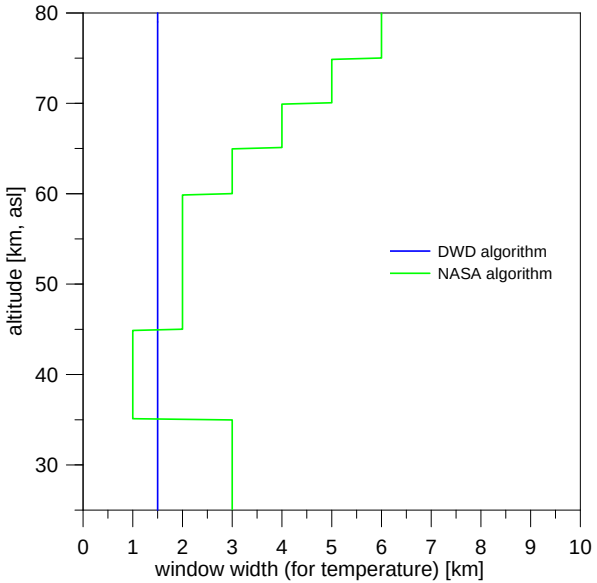

Fig. 5. Range resolution for the NASA and DWD temperature processing algorithms.

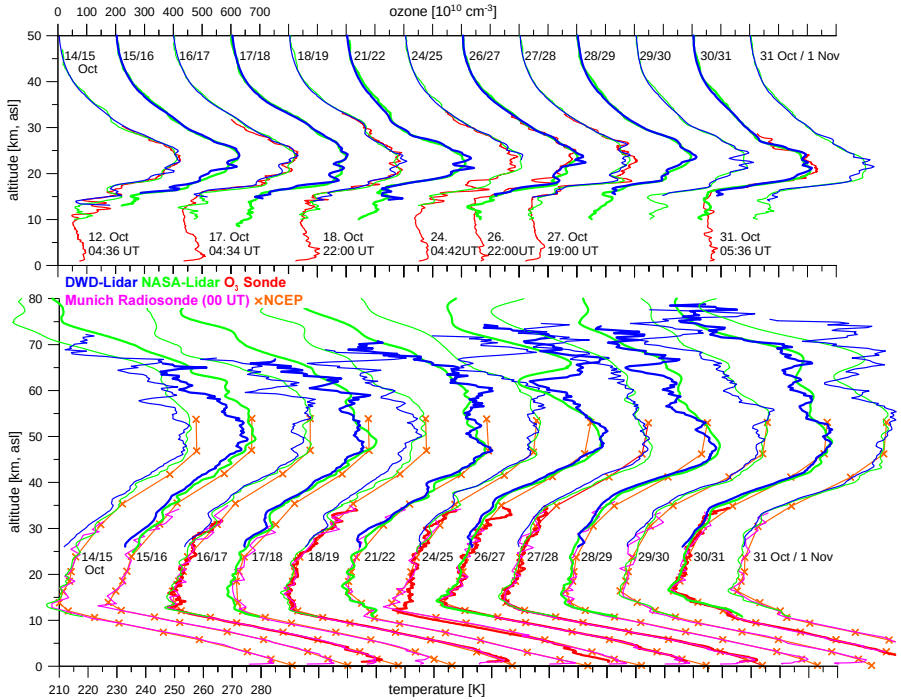

Fig. 6. Top: Ozone profiles measured between 12 October 2005 and 1 November 2005 at Hohenpeissenberg by DWD lidar (blue), NASA lidar (green), and by Hohenpeissenberg ozonesondes (red). The lidar profiles are nightly means. For the sondes, the launch time is given in UT (universal time =local time – 1 h). Bottom: Same, but for temperature profiles measured by DWD Lidar (blue), NASA lidar (green), Hohenpeissenberg ozonesondes (red), and Munich radiosondes (magenta, 23:00 UT launch time). Also shown is the 00:00 UT temperature profile (orange) interpolated from the daily 12:00 UT analyses of the US National Centers for Environmental Prediction (NCEP).

AMTD
2, 37–86, 2009

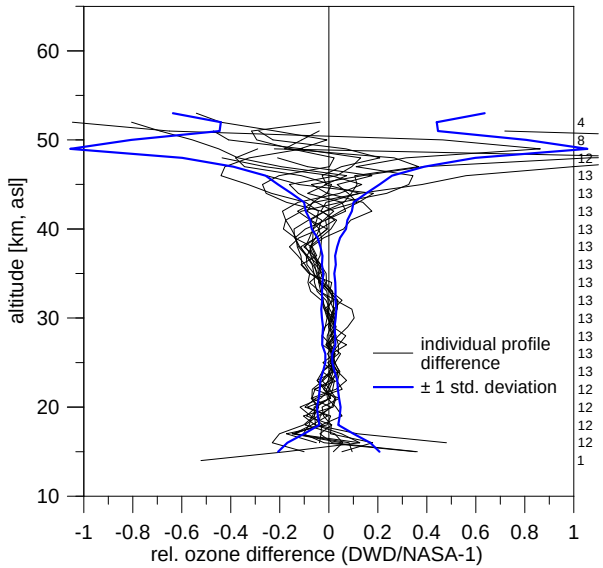

Fig. 7. Relative difference between nightly mean ozone number density from DWD and NASA lidar. The NASA profiles serve as the reference. The blue lines give plus and minus one standard deviation, offset from the zero line. Numbers on the right give the number of available ozone difference profiles.

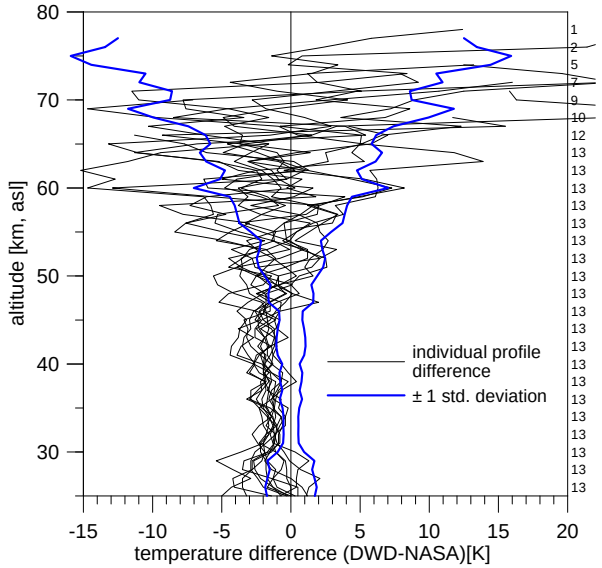

Fig. 8. Same as Fig. 7, but for the absolute temperature difference between DWD and NASA lidar. Note the different altitude range, from 25 to 80 km, instead of from 15 to 65 km for the relative ozone differences in Fig. 7. Numbers on the right give the number of available temperature difference profiles.

AMTD
2, 37–86, 2009

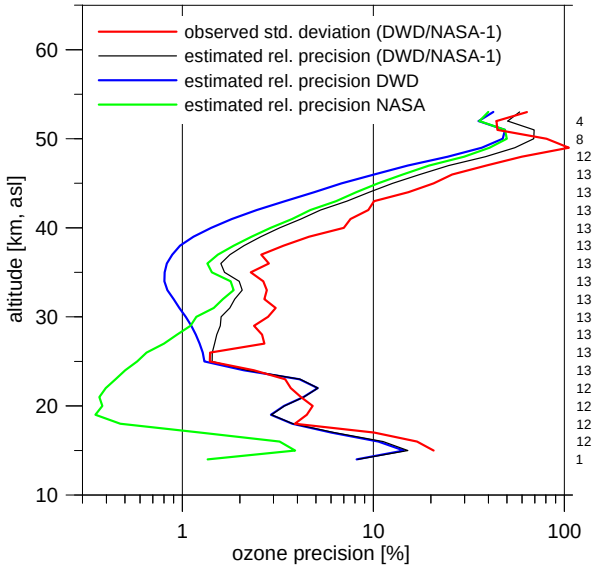

Fig. 9. Relative precision estimates ΔX_i for ozone profiles from DWD (blue line) and NASA lidar (green line) during HOPE. Black line: Precision estimate $\Delta_{\text{est}}(dX)$ for the ozone relative difference dX. Red line: Observed standard deviation $\sigma_{\text{meas}}(dX)$ of relative ozone differences during HOPE (same as blue curve in Fig. 7). Numbers on the right give the number of ozone difference profiles during HOPE.

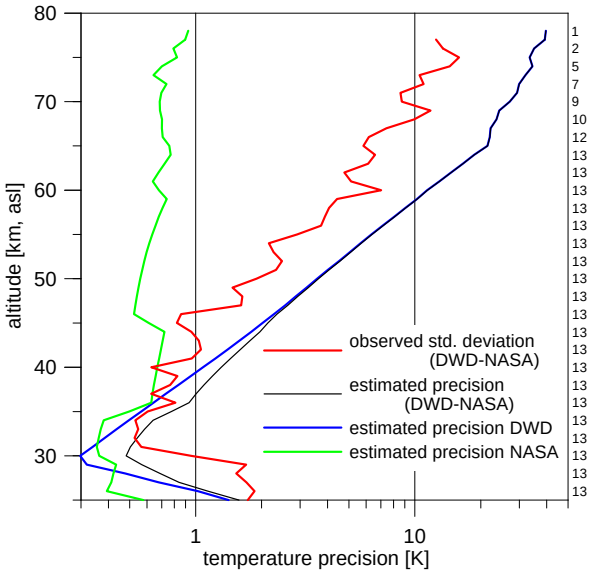

Fig. 10. Same as Fig. 9, but for estimated temperature precision ΔX_i for DWD (blue line) and NASA (green line) lidar, for the estimated precision $\Delta_{est}(dX)$ of temperature differences between the DWD and NASA lidars (black line), and for the observed standard deviation $\sigma_{meas}(dX)$ of temperature differences (red line = same as blue curve in Fig. 8). Numbers on the right give the number of available temperature difference profiles. Note the different altitude range, from 25 to 80 km, instead of from 15 to 65 km for ozone in Fig. 9.

AMTD
2, 37–86, 2009

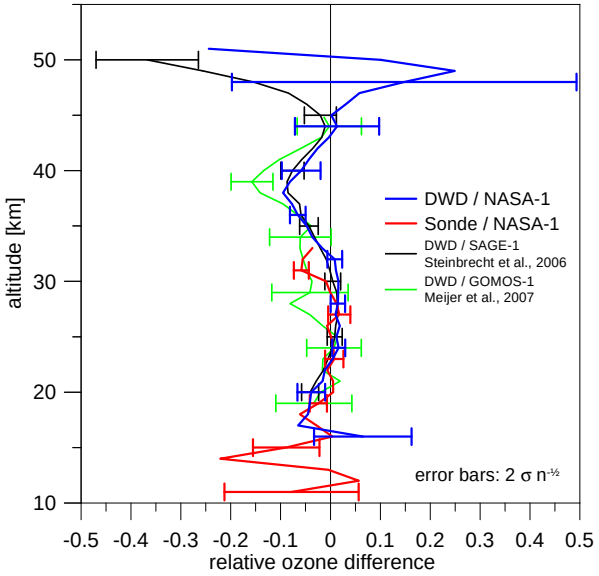

Fig. 11. Average relative ozone difference profiles. Blue: Between DWD and NASA lidars during HOPE. Red: Between ozonesondes and NASA lidar during HOPE. Black: Average difference between DWD lidar and SAGE II (version 6.2) over the period 1987 to 2005 (Steinbrecht et al., 2006). Green: Average difference between DWD lidar and GOMOS (version 6.0f, updated from Meijer et al., 2004). Error bars: Two standard errors of the mean.

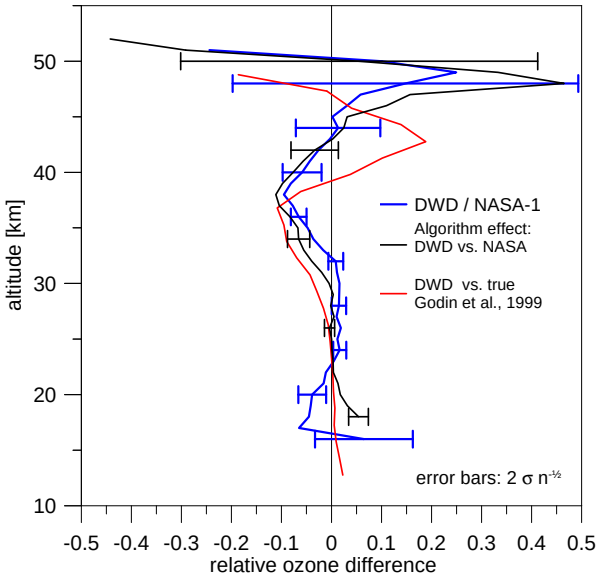

Fig. 12. Blue line: Observed relative ozone difference between DWD and NASA lidar during HOPE, same as in Fig. 11. Black line: Relative ozone difference between NASA lidar return signals processed by DWD algorithm and processed by NASA algorithm. Red line: Bias of the DWD algorithm in the NDSC algorithm intercomparison (Godin et al., 1999). Error bars are two standard errors of the mean.

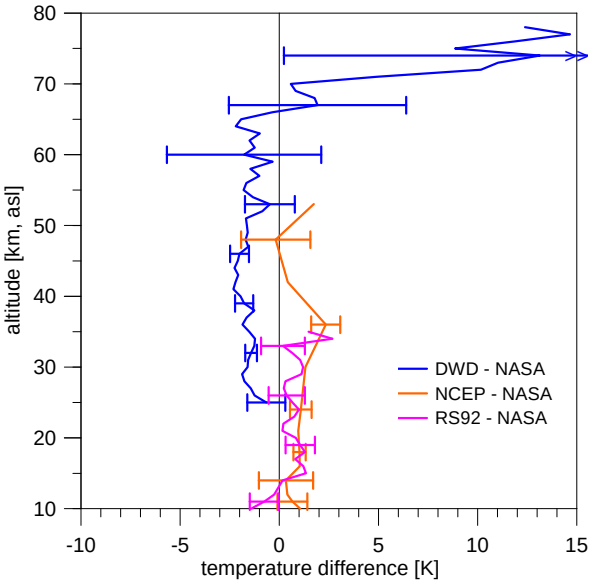

Fig. 13. Average temperature differences during HOPE. Blue: Between DWD and NASA lidar. Orange: Between NCEP operational analyses and NASA lidar. Magenta: Between Munich Vaisala RS92 radiosondes and NASA lidar. Error bars: Two standard errors of the mean.

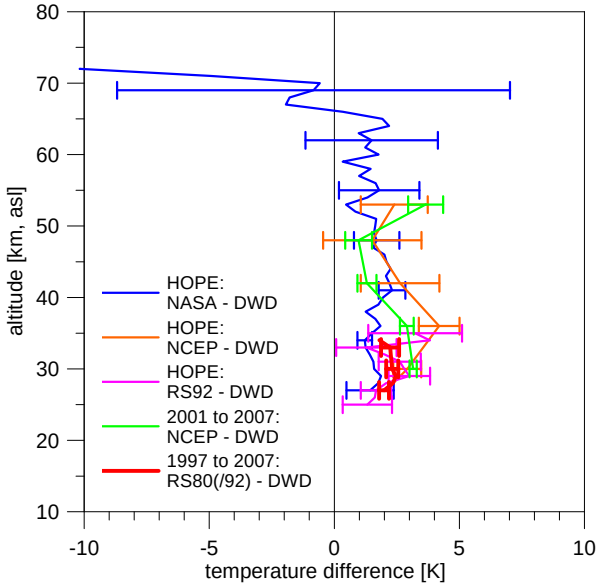

Fig. 14. Similar to Fig. 13 but for average temperature differences to the DWD lidar. Blue: NASA minus DWD lidar during HOPE. Orange: NCEP minus DWD lidar during HOPE. Magenta: Munich radiosondes (Vaisala RS92) minus DWD lidar during HOPE. Green: NCEP minus DWD lidar over the period July 2001 to October 2007 (about 600 cases). Red: Hohenpeissenberg sondes minus DWD lidar, over the period October 1997 to October 2007 (about 300 cases, sondes launched within 10 h of the lidar measurement). Error bars: Two standard errors of the mean.

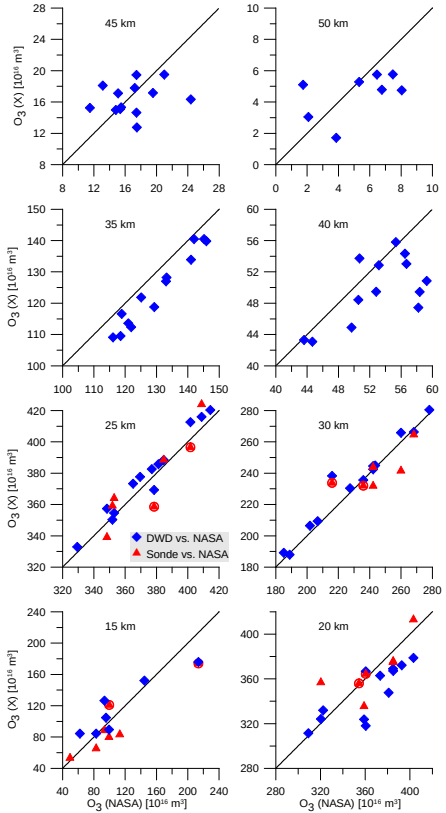

Fig. 15. Scatter plots of ozone number density during HOPE at selected altitude levels. Ozone measured by DWD lidar (blue diamonds), and ozonesondes (red triangles) is plotted against ozone from the NASA lidar. Ozonesondes were launched within 6 h of the lidar measurement, execpt for the two sonde points indicated by a red circle around the red triangle (12 and 24 October 2005 launches). Each data point represents an ozone value from a sonde and/ or nightly mean ozone from a lidar.

AMTD
2, 37–86, 2009

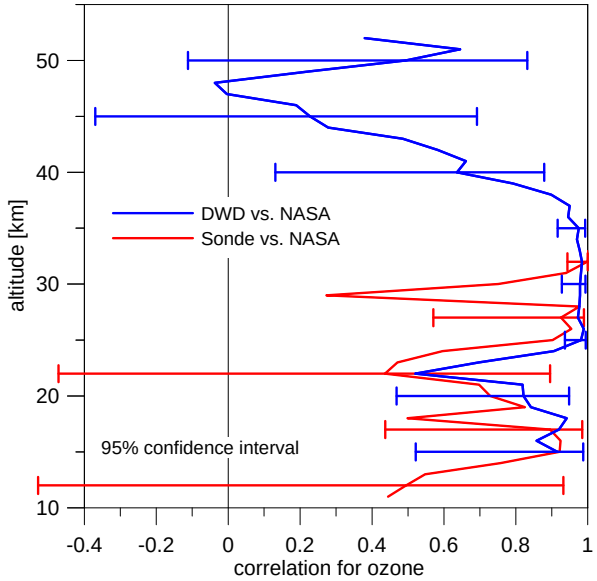

Fig. 16. Linear correlation coefficient between ozone measured by DWD lidar and ozone from the NASA lidar(blue line), or between ozonesondes (red line) and NASA lidar. Error bars give the 95% confidence interval.

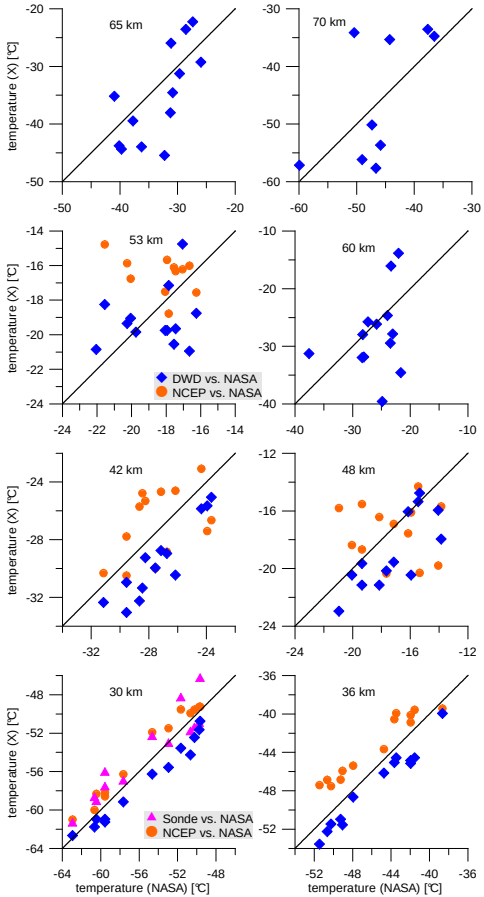

Fig. 17. Scatter plots for temperature during HOPE at selected altitudes. Temperatures from DWD lidar (blue diamonds), Munich radiosondes (magenta triangles), and NCEP (orange circles) are plotted against temperature from the NASA lidar.

AMTD
2, 37–86, 2009

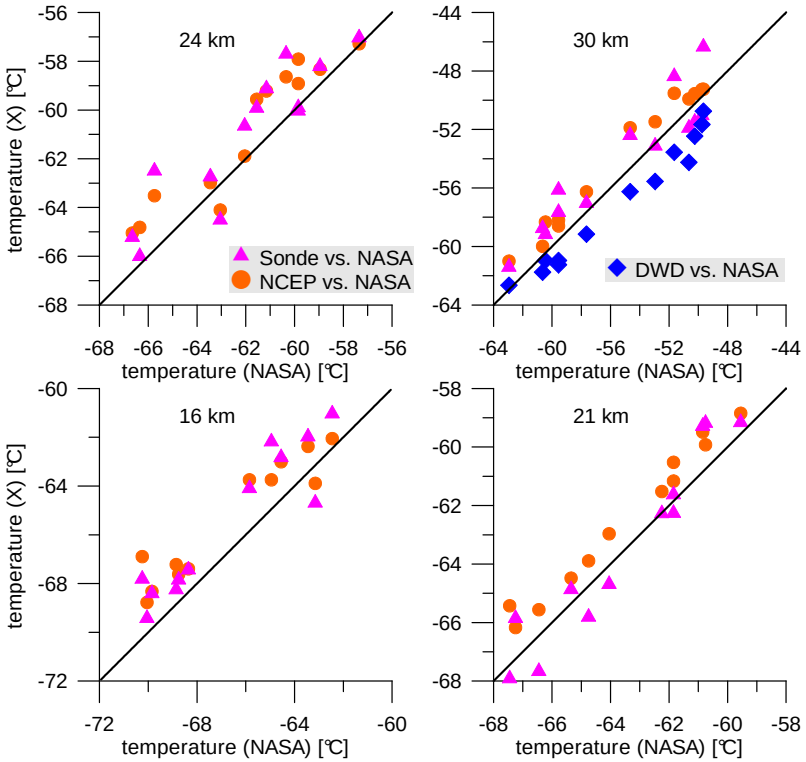

Fig. 18. Same as Fig. 17, but for altitudes between 16 and 30 km. The DWD lidar does not report temperature below about 27 km.

AMTD
2, 37–86, 2009

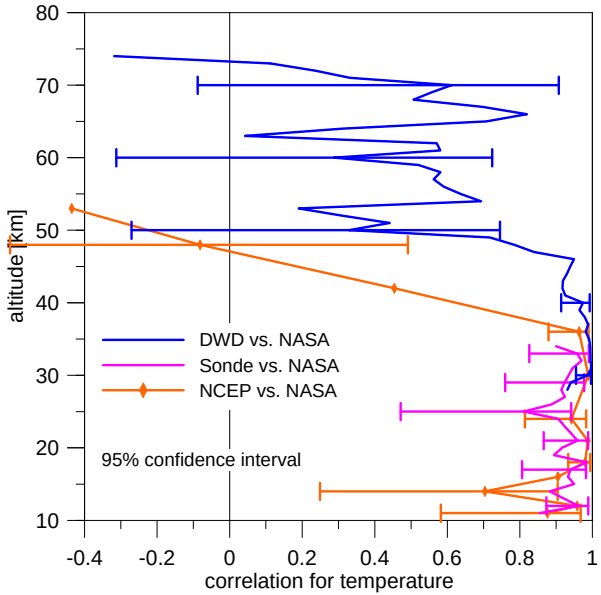

Fig. 19. Correlation coefficient between temperature from the NASA lidar and temperature from DWD lidar (blue line), Munich radiosondes (magenta line), and NCEP (orange line). Error bars give the 95% confidence interval.

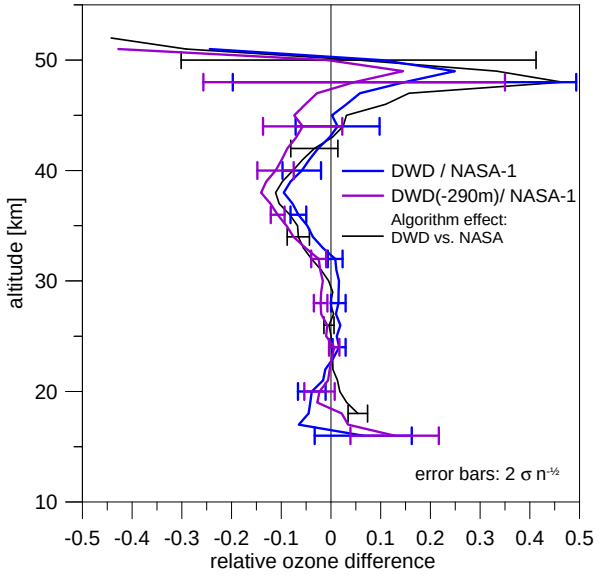

Fig. 20. Relative ozone difference during HOPE. Violet: Between DWD lidar, corrected for 290 m altitude offset, and NASA lidar. Blue: Between DWD and NASA lidar, same as in Figs. 11 and 12. Black line: Difference between DWD and NASA algorithms, same as in Fig. 12. Error bars: Two standard errors of the mean.

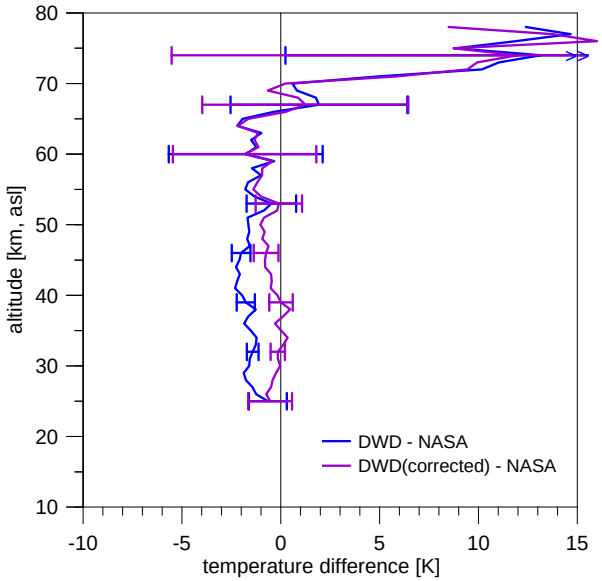

Fig. 21. Temperature difference during HOPE. Violet: Between DWD lidar, corrected for 290 m altitude offset and $g(z)$, and NASA lidar. Blue: Between DWD and NASA lidar, same as in Figs. 13 and 14. Error bars: Two standard errors of the mean.

AMTD
2, 37–86, 2009